

Possible way to achieve anomalous valley Hall effect by piezoelectric effect in a GdCl₂ monolayerSan-Dong Guo ^{1,*}, Jing-Xin Zhu,¹ Wen-Qi Mu,¹ and Bang-Gui Liu ^{2,3}¹*School of Electronic Engineering, Xi'an University of Posts and Telecommunications, Xi'an 710121, People's Republic of China*²*Beijing National Laboratory for Condensed Matter Physics, Institute of Physics, Chinese Academy of Sciences, Beijing 100190, People's Republic of China*³*School of Physical Sciences, University of Chinese Academy of Sciences, Beijing 100190, People's Republic of China*

(Received 7 October 2021; revised 6 December 2021; accepted 7 December 2021; published 23 December 2021)

Ferrovalley materials can achieve manipulation of the valley degree of freedom with intrinsic spontaneous valley polarization introduced by their intrinsic ferromagnetism. A good ferrovalley material should possess perpendicular magnetic anisotropy (PMA), the valence band maximum (VBM) or conduction band minimum at valley points, strong ferromagnetic (FM) coupling, and proper valley splitting. In this work, the monolayer GdCl₂ is proposed as a potential candidate material for valleytronic applications using the first-principles calculations. It is proved that monolayer GdCl₂ is a FM semiconductor with the easy axis along the out-of-plane direction and strong FM coupling. A spontaneous valley polarization with a valley splitting of 42.3 meV is produced due to its intrinsic ferromagnetism and spin-orbit coupling. Such valley splitting is larger than the thermal energy at room temperature, suggesting the possibility of room-temperature device operations. Although the VBM of unstrained monolayer GdCl₂ is away from the valley points, a very small compressive strain (about 1%) can make the VBM move to the valley points. We propose a possible way to realize the anomalous valley Hall effect in monolayer GdCl₂ using the piezoelectric effect, not an external electric field, namely, the piezoelectric anomalous valley Hall effect. This phenomenon could be classified as piezovalletronics, being similar to piezotronics and piezophotonics. The only independent piezoelectric strain coefficient d_{11} is -2.708 pm/V, which is comparable to that of the classical bulk piezoelectric material α -quartz ($d_{11} = 2.3$ pm/V). The biaxial in-plane strain and electronic correlation effects are considered to confirm the reliability of our results. Finally, monolayer GdF₂ is predicted to be a ferrovalley material with dynamic and mechanical stabilities, PMA, the VBM at the valley points, strong FM coupling, valley splitting of 47.6 meV, and d_{11} of 0.584 pm/V. Our work provides a possible way to achieve the anomalous valley Hall effect using the piezoelectric effect, which may stimulate further experimental works related to valleytronics.

DOI: [10.1103/PhysRevB.104.224428](https://doi.org/10.1103/PhysRevB.104.224428)**I. INTRODUCTION**

Rather than spin and charge, carriers in crystals are endowed with the valley degree of freedom, which is useful to process information and perform logic operations (valleytronics) [1–6]. Two or more local energy extremes in the conduction band or valence band, which are degenerate but inequivalent at the inequivalent k points in momentum space, are needed for a valley material. To realize applications of valleytronics, the electrons or holes in different valleys must be selectively produced or manipulated. Although the possibility to achieve manipulation of the valley degree of freedom has been proposed for certain three-dimensional (3D) materials [7], the field of valleytronics is truly flourishing with the advent of two-dimensional (2D) materials.

The reduction in dimensionality of 2D materials results in the space inversion symmetry often being eliminated in 2D structures, allowing these materials to become piezoelectric [8], which is also very important for valleytronics described by Berry curvature $\Omega(k)$. In 2D hexagonal systems with broken space inversion symmetry, the Berry curvature

in the K and $-K$ valleys will be nonzero along the out-of-plane direction, and the Berry curvatures of the two valleys have opposite signs. If the time reversal symmetry is also broken, their absolute values are no longer identical, and the valley contrasting feature will be induced. Under an in-plane longitudinal electric field E , the Bloch electrons in these 2D systems will acquire an anomalous Hall velocity v because $v \sim E \times \Omega(k)$ [9], and then the anomalous valley Hall effect will be produced, which can be achieved in ferrovalley materials [10]. Many ferrovalley materials have been predicted, such as $2H$ -VSe₂ [10], CrSi₂X₄ ($X = N$ and P) [11], VAgP₂Se₆ [12], LaBr₂ [13,14], VSi₂P₄ [15], NbX₂ ($X = S$ and Se) [16], Nb₃I₈ [17], TiVI₆ [18]. It is a natural idea to induce an in-plane longitudinal electric field E with an applied uniaxial in-plane strain using the piezoelectric effect, and then the anomalous valley Hall effect can be produced, which is illustrated in Fig. 1.

To well achieve the piezoelectric anomalous valley Hall effect (PAVHE), a 2D material should meet the following conditions: (1) strong ferromagnetic (FM) coupling with perpendicular magnetic anisotropy (PMA), which is important not only for FM order but also for valley behavior; (2) an appropriate energy band gap and valley splitting, which should be large enough to overcome the thermal noise; and (3) the

*Corresponding author: sandongyuwang@163.com

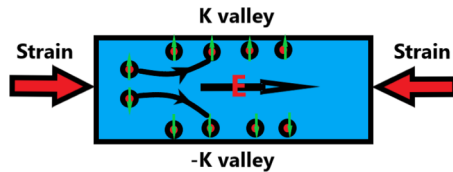


FIG. 1. Sketch of the anomalous valley Hall effect under an in-plane longitudinal electric field E , where E is induced with uniaxial strain using the piezoelectric effect. Upward arrows and downward arrows represent spin-up and spin-down carriers, respectively. Only one edge of the sample can accumulate the charge carriers; another edge will accumulate them when the magnetization orientation is reversed.

pure in-plane piezoelectric effect with only d_{11} , which means only an in-plane longitudinal electric field. Recently, a kind of exotic 2D ferromagnetic semiconductor, GdX_2 ($X = \text{Cl, Br, and I}$), based on rare-earth ions with f electrons was predicted to have a large magnetization with a high Curie temperature beyond 220 K [19,20]. Monolayer GdI_2 is predicted as a promising candidate material for valleytronic applications because it is spontaneously valley polarized with a giant splitting of 149 meV [21]. However, GdI_2 possesses in-plane magnetic anisotropy, not PMA [19,20]. Among GdX_2 ($X = \text{Cl, Br, and I}$) monolayers, the easy axis of only monolayer GdCl_2 is along the out-of-plane direction [20]. Monolayer GdCl_2 has the $P\bar{6}m2$ point-group symmetry, which means that only the independent d_{11} is nonzero.

In light of PMA and independent d_{11} , monolayer GdCl_2 is likely to be a potential ferromagnetic material to realize PAVHE. In this work, we investigate the valley physics and piezoelectric properties of monolayer GdCl_2 using first-principles calculations. Monolayer GdCl_2 exhibits a pair of valleys in the valance band at the K and $-K$ points with a valley splitting of 42.3 meV due to its intrinsic ferromagnetism and spin-orbit coupling (SOC). The predicted d_{11} is -2.708 pm/V, which is comparable to that of α -quartz ($d_{11} = 2.3$ pm/V). To confirm the reliability of our results, the biaxial in-plane strain and electronic correlation effects on valley physics and piezoelectric properties are considered. Finally, monolayer GdF_2 is predicted to be a likely potential ferromagnetic material. Our work provides potential 2D valleytronic materials to achieve PAVHE to develop high-performance and controllable valleytronics.

The rest of this paper is organized as follows. In the next section, we give our computational details and methods. In the following sections, we present the structure and stability, electronic structure and valley Hall effect, and piezoelectric properties of monolayer GdCl_2 , along with the strain and electronic correlation effects on its valleytronic and piezoelectric properties. Finally, we provide a discussion and conclusions in the last section.

II. COMPUTATIONAL DETAILS

First-principles calculations with spin polarization are performed within density functional theory [22], as implemented in the Vienna Ab initio Simulation Package (VASP) [23–25] within the projector augmented-wave method. The

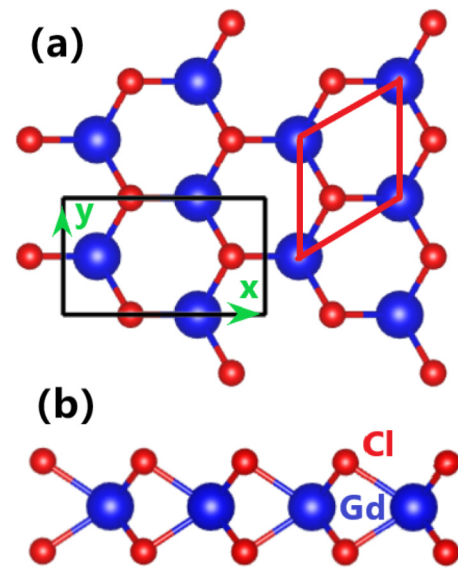


FIG. 2. The (a) top view and (b) side view of the crystal structure of monolayer GdCl_2 . The red and black frames represent the rhombus primitive cell and rectangular supercell. The rectangular supercell is used to calculate the piezoelectric stress coefficients, whose width and height are defined as the x and y directions, respectively.

generalized gradient approximation (GGA) in the form of the Perdew-Burke-Ernzerhof functional [26] is used for the exchange-correlation interactions. The kinetic energy cutoff is set to 500 eV, and the total energy convergence criterion 10^{-8} eV is used. The optimized convergence criterion for atomic coordinates is less than 0.0001 eV \AA^{-1} for the force on each atom. The vacuum space is set to more than 18 \AA to avoid adjacent interactions. An $18 \times 18 \times 1$ Monkhorst-Pack k -point mesh is used to sample the Brillouin zone to calculate electronic structures and elastic properties, and a $10 \times 20 \times 1$ Monkhorst-Pack k -point mesh is used for piezoelectric calculations. To account for the localized nature of $4f$ orbitals of Gd atoms, a Hubbard correction U_{eff} is employed within the rotationally invariant approach proposed by Dudarev

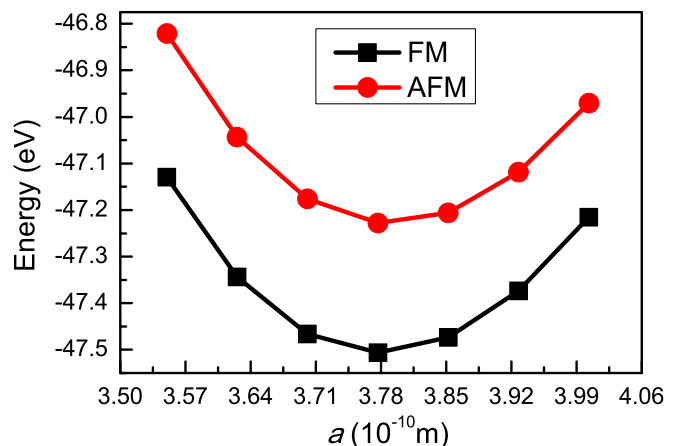


FIG. 3. Calculated energy of the AFM state and the FM state of monolayer GdCl_2 as a function of lattice constants a with a rectangular supercell.

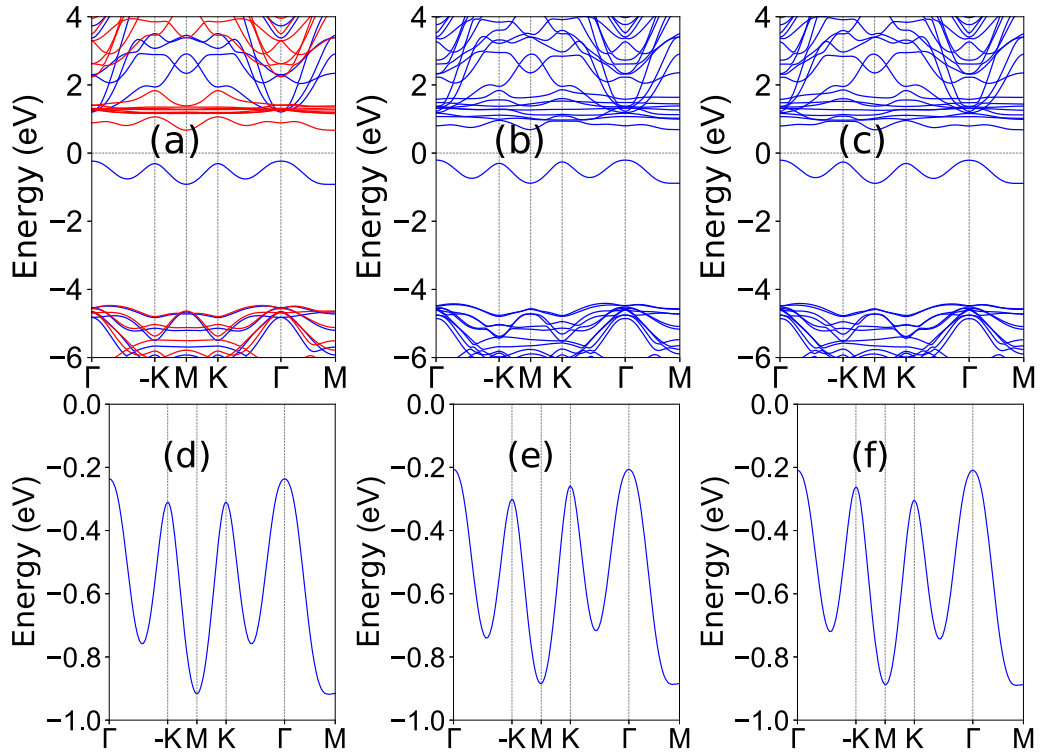


FIG. 4. The band structure of monolayer GdCl₂ (a) without SOC and (b) and (c) with SOC for the magnetic moment of Gd along the positive and negative z directions (out of plane), respectively. (d)–(f) Enlarged views of the valence bands near the Fermi level for (a)–(c).

et al. [27], where U_{eff} is set as 4, 5, and 8 eV [19,20] for monolayer GdCl₂, GdBr₂, and GdI₂, respectively. The SOC is incorporated for self-consistent energy and band structure calculations. The elastic stiffness tensors C_{ij} are calculated using the strain-stress relationship with GGA, and the piezoelectric stress tensors e_{ij} are determined using the density functional perturbation theory (DFPT) method [28] with GGA. The 2D elastic coefficients C_{ij}^{2D} and piezoelectric stress coefficients e_{ij}^{2D} have been renormalized by $C_{ij}^{2D} = L_z C_{ij}^{3D}$ and $e_{ij}^{2D} = L_z e_{ij}^{3D}$, where L_z is the length of the unit cell along the z direction. Within the finite-displacement method, the interatomic force constants (IFCs) of monolayer GdF₂ are

calculated based on the $5 \times 5 \times 1$ supercell with the FM ground state. Based on the harmonic IFCs, the phonon dispersion spectrum of monolayer GdF₂ is obtained using the PHONOPY code [29].

III. STRUCTURE AND STABILITY

Monolayer GdCl₂ belongs to the hexagonal crystal system with $2H$ -MoS₂-type structure, which contains one Gd atomic layer sandwiched by two Cl atomic layers (see Fig. 2). The corresponding point group is $P\bar{6}m2$ with broken inversion symmetry. The magnetic ground state of monolayer GdCl₂ is

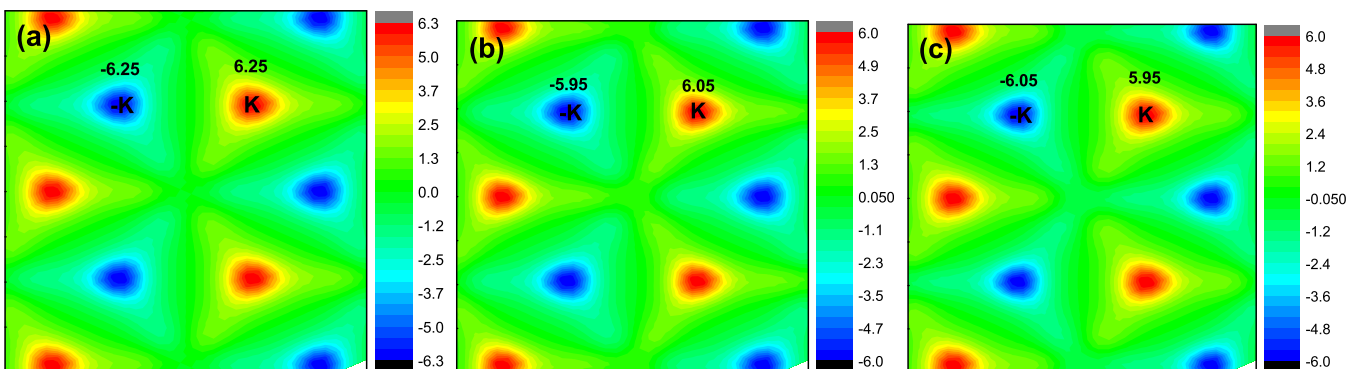


FIG. 5. Calculated Berry curvature distribution of monolayer GdCl₂ in the 2D Brillouin zone (a) without SOC and (b) and (c) with SOC for the magnetic moment of Gd along the positive and negative z directions (out of plane), respectively.

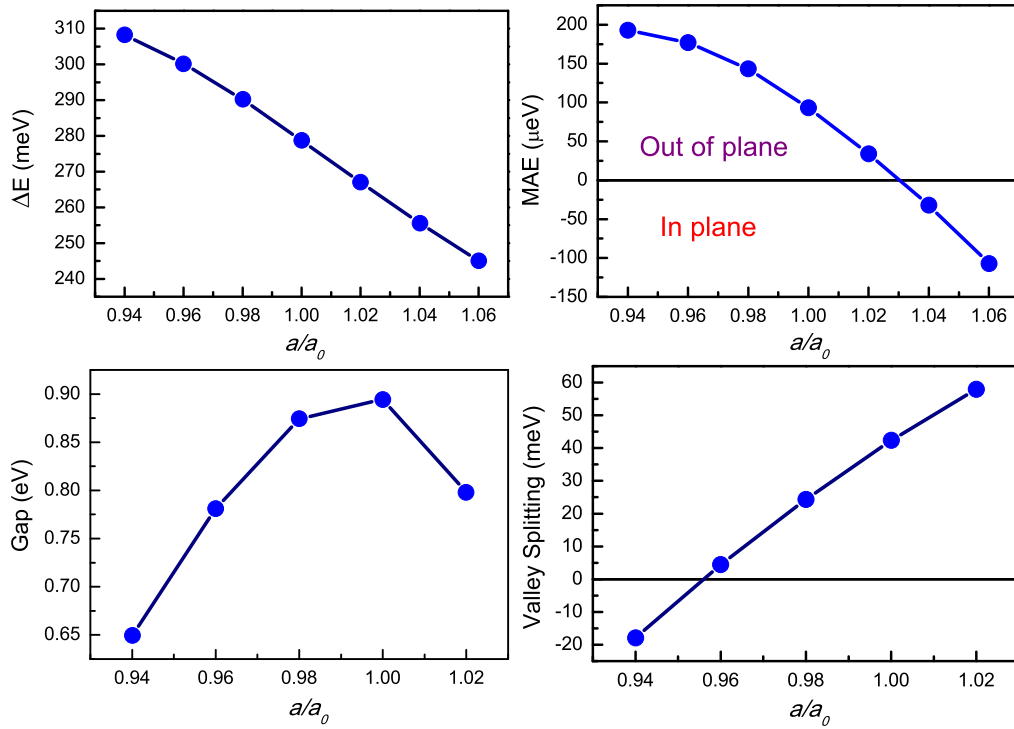


FIG. 6. Top left: The energy difference between the AFM and FM states ΔE . Top right: MAE. Bottom left: Energy band gap. Bottom right: Valley splitting as a function of the applied biaxial strain a/a_0 for monolayer GdCl_2 .

determined by comparing the energies of antiferromagnetic (AFM) and FM states with a rectangular supercell, which is shown in Fig. 3. The calculated results show that the FM order is the most stable magnetic state, and the optimized lattice constant with FM order is 3.78 Å, which is consistent with the reported value [20]. Magnetic anisotropy plays an important role in realizing long-range magnetic ordering in 2D materials, which can be described by the magnetic anisotropy energy (MAE). Monolayer GdBr_2 and GdI_2 possess in-plane magnetic anisotropy [19,20]. This means that the spin orientations of Gd atoms can be random, and it is difficult to realize the long-range magnetic ordering without external field. However, the easy axis of monolayer GdCl_2 is along the out-of-plane direction [20]. By considering SOC interaction, the MAE of monolayer GdCl_2 is calculated as the difference between the in-plane and out-of-plane magnetization stability energies, and the corresponding value is 93 $\mu\text{eV}/\text{Gd}$. The thermal and dynamic stabilities of monolayer GdCl_2 have

been proved by *ab initio* molecular dynamics simulations and phonon dispersion [20]. It is also important to check the mechanical stability of monolayer GdCl_2 by calculating the elastic constants. Using Voigt notation, the elastic tensor C with the $P6m2$ point-group symmetry for 2D materials can be reduced to

$$C = \begin{pmatrix} C_{11} & C_{12} & 0 \\ C_{12} & C_{11} & 0 \\ 0 & 0 & (C_{11} - C_{12})/2 \end{pmatrix}. \quad (1)$$

The calculated results show that C_{11} and C_{12} are 45.95 and 13.53 N m^{-1} , respectively. The calculated C_{ij} satisfy the Born criteria for mechanical stability [30], $C_{11} > 0$ and $C_{11} - C_{12} > 0$, which confirms the mechanical stability of monolayer GdCl_2 . Due to hexagonal symmetry, monolayer GdCl_2 is mechanically isotropic. The 2D Young's moduli C^{2D} , shear modulus G^{2D} , and Poisson's ratios ν^{2D} can simply be

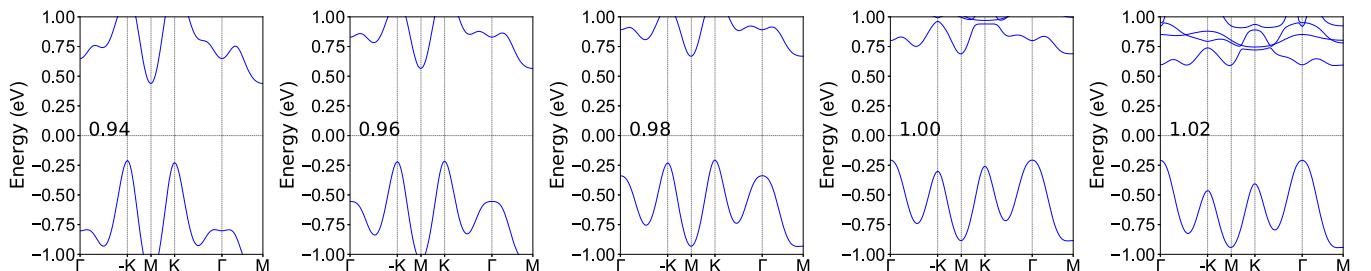


FIG. 7. The energy band structures of monolayer GdCl_2 with a/a_0 from 0.94 to 1.02 using GGA+SOC.

TABLE I. For monolayer GdX_2 ($X = \text{F}, \text{Cl}, \text{Br}, \text{and I}$), the elastic constants C_{ij} (in N m^{-1}); the piezoelectric stress coefficients e_{11} , with the electronic part e_{11e} and ionic part e_{11i} (in 10^{-10} C/m); and the piezoelectric strain coefficients d_{11} (in pm/V).

Name	C_{11}	C_{12}	e_{11e}	e_{11i}	e_{11}	d_{11}
GdF_2	73.87	19.61	1.365	-1.048	0.317	0.584
GdCl_2	45.95	13.53	1.028	-1.906	-0.878	-2.708
GdBr_2	40.46	11.68	0.847	-1.742	-0.895	-3.110
GdI_2	35.49	10.09	0.658	-1.356	-0.698	-2.748

expressed as [30]

$$C^{2D} = \frac{C_{11}^2 - C_{12}^2}{C_{11}}, \quad (2)$$

$$G^{2D} = C_{66} = \frac{C_{11} - C_{12}}{2}, \quad (3)$$

$$\nu^{2D} = \frac{C_{12}}{C_{11}}. \quad (4)$$

The calculated Young's moduli C^{2D} , shear modulus G^{2D} , and Poisson's ratio ν are 41.97 N m^{-1} , 16.21 N m^{-1} , and 0.295 , respectively. C^{2D} is less than that of graphene (340 N m^{-1}) [31], which indicates that monolayer GdCl_2 can be easily tuned by strain, making it favorable for novel flexible piezotronics.

IV. ELECTRONIC STRUCTURE AND VALLEY HALL EFFECT

The electronic configuration of an isolated Gd atom is $4f^7 5d^1 6s^2$. For monolayer GdCl_2 , two electrons of one Gd atom are transferred to the six neighboring I atoms, and the electronic configuration of Gd becomes $4f^7 5d^1$, which will introduce an $8\mu_B$ magnetic moment. The calculated magnetic moment of Gd is $7.463\mu_B$, and the total magnetic moment per unit cell is $8\mu_B$. The spin-polarized band structure of monolayer GdCl_2 without SOC is shown in Fig. 4. The calculated results show that monolayer GdCl_2 is a semiconductor with an indirect band gap of 0.91 eV . The valence band maximum (VBM) and conduction band minimum (CBM) are provided by the majority spins and minority spins, and they locate

at the Γ and M high-symmetry points, respectively. This makes monolayer GdCl_2 a bipolar magnetic semiconductor, which can generate 100% spin-polarized currents with the inverse spin-polarization direction for electron or hole doping. It is clearly seen that the energy extremes of the K and $-K$ high-symmetry points are degenerate in the valence band [Fig. 4(d)], and monolayer GdCl_2 is a potential ferrovalley material.

The band structures of monolayer GdCl_2 with SOC for a magnetic moment of Gd along the positive and negative z directions (out of plane) are also plotted in Fig. 4. When the SOC is included, the degeneracy between the K and $-K$ valley states is removed in the valence band, and a spontaneous valley polarization is induced with valley splitting of 42.3 meV , which is higher than or similar to those of reported ferrovalley materials, such as VAgP_2Se_6 (15 meV) [12], LaBr_2 (33 meV) [13,14], TiVI_6 (22 meV) [18], VSi_2P_4 (49.4 meV) [15], and $2H\text{-VSe}_2$ (89 meV) [10]. It is found that the energy of the K valley state is higher than that of the $-K$ valley [Fig. 4(e)]. It is interesting that an external magnetic field can tune the valley polarization of monolayer GdCl_2 . By reversing the magnetization of Gd atoms, the spin and valley polarizations can be flipped simultaneously, and the energy of the $-K$ valley becomes higher than that of the K valley [Fig. 4(f)]. These results mean that manipulating the magnetization direction is an efficient way to tune the valley properties of monolayer GdCl_2 . Furthermore, the band related to valley properties is separated well from other energy bands. Although the VBM of monolayer GdCl_2 occurs at the Γ point, the K and $-K$ valleys are still well defined and not far in energy. In fact, a very small compressive strain (about 1%) can change the VBM from Γ to the $K/-K$ point (see the next section). As is well known, the GGA overestimates the lattice constants of materials, and the VBM of monolayer GdCl_2 may intrinsically locate at the $K/-K$ point.

The combined effects of the intrinsic magnetic exchange field and strong SOC give rise to the spontaneous valley polarization. When the spin polarization is performed without SOC, the spin-up and spin-down states are completely split by the magnetic exchange interaction, but the energy extremes of the K and $-K$ high-symmetry points are degenerate in the valence band. When the magnetic exchange interaction is absent, SOC can still induce spin nondegeneracy in both the

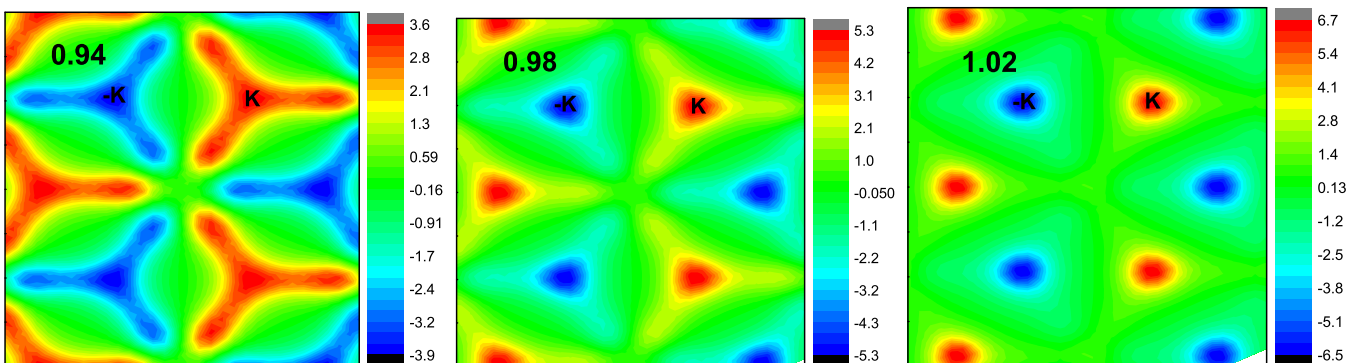


FIG. 8. Calculated Berry curvature distribution of monolayer GdCl_2 in the 2D Brillouin zone with a/a_0 being 0.94 , 0.98 , and 1.02 using GGA+SOC.

K and $-K$ valleys due to missing spatial inversion symmetry, but the K and $-K$ valleys are energetically degenerate with opposite spins because of the existing time reversal symmetry. Briefly, combined with a high Curie temperature (224 K) [20] and PMA, GdCl_2 is an ideal ferrovalley material for the valleytronic devices.

The valley Hall effect can be described by Berry curvature, and a nonzero Berry curvature along the out-of-plane direction can be attained in the K and $-K$ valleys for hexagonal systems with broken space inversion symmetry. With the missing time reversal symmetry, the valley contrasting feature can be produced. To study these properties of monolayer GdCl_2 , the Berry curvature is calculated directly from the calculated wave functions by using the VASPBERRY code, which is based on Fukui's method [32]. The calculated Berry curvature distributions of monolayer GdCl_2 in the 2D Brillouin zone without SOC and with SOC for the magnetic moment of Gd along the positive and negative z directions are shown in Fig. 5. Without SOC, the Berry curvatures of the K and $-K$ valleys have opposite signs, and the absolute values are the same. When the SOC is included, the absolute values of the Berry curvatures of the K and $-K$ valleys are no longer identical, which shows typical valley contrasting properties. It is also found that the numerical values between the K and $-K$ valleys overturn when the magnetic moment of Gd changes from the positive to negative z direction.

V. PIEZOELECTRIC PROPERTIES

Monolayer GdCl_2 with the $P\bar{6}m2$ point-group symmetry lacks inversion symmetry, but the reflectional symmetry across the xy plane still holds. This means that only e_{11} or d_{11} with defined x and y directions in Fig. 2 is nonzero. This is the same with ones of MoS_2 monolayer but is different from those of the Janus monolayer MoSSe with additional e_{31}/d_{31} [33]. For 2D materials, considering only the in-plane strain and stress [8,33–40], the piezoelectric stress and strain tensors using Voigt notation can be reduced to

$$\begin{pmatrix} e_{11} & -e_{11} & 0 \\ 0 & 0 & -e_{11} \\ 0 & 0 & 0 \end{pmatrix}, \quad (5)$$

$$\begin{pmatrix} d_{11} & -d_{11} & 0 \\ 0 & 0 & -2d_{11} \\ 0 & 0 & 0 \end{pmatrix}. \quad (6)$$

When a uniaxial in-plane strain is imposed, the in-plane piezoelectric polarization ($e_{11}/d_{11} \neq 0$) can be induced. However, with an applied biaxial in-plane strain, the in-plane piezoelectric response will be suppressed ($e_{11}/d_{11} = 0$). The only independent d_{11} can be calculated by $e_{ik} = d_{ij}C_{jk}$:

$$d_{11} = \frac{e_{11}}{C_{11} - C_{12}}. \quad (7)$$

We use the orthorhombic supercell (in Fig. 2) to calculate e_{11} of monolayer GdCl_2 with the DFPT method. The calculated e_{11} is -0.878×10^{-10} C/m, with the ionic part being -1.906×10^{-10} C/m and the electronic part being 1.028×10^{-10} C/m. The electronic and ionic polarizations

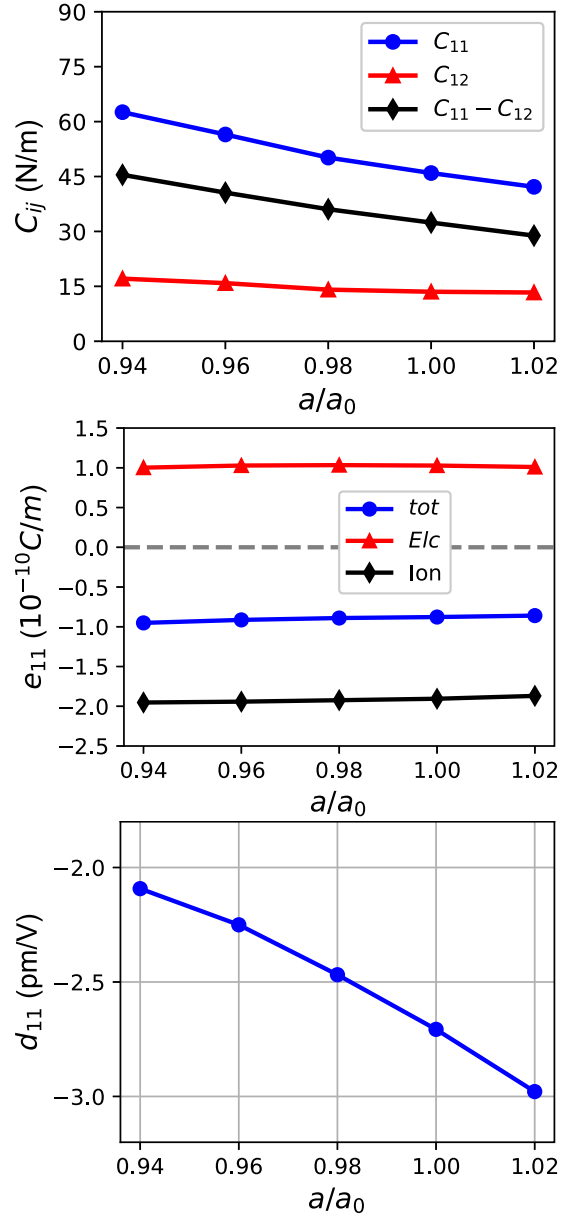


FIG. 9. For monolayer GdCl_2 , the elastic constants C_{ij} ; the piezoelectric stress coefficient e_{11} , along with the ionic contribution and electronic contribution; and the piezoelectric strain coefficient d_{11} with the application of biaxial strain (0.94 to 1.02).

have opposite signs, and the ionic contribution dominates the in-plane piezoelectricity. This is different from monolayer MoS_2 , in which the electronic and ionic contributions have the same sign and the electronic part dominates e_{11} [40]. Based on Fig. 7 below, d_{11} can be calculated from previously calculated C_{ij} and e_{11} . The calculated d_{11} is -2.708 pm/V, which is comparable to that of α -quartz ($d_{11} = 2.3$ pm/V). GdX_2 ($X = \text{Br}$ and I) monolayers have been predicted [19,20], and they possess in-plane magnetic anisotropy. Here, we use the GGA + U_{eff} ($U_{\text{eff}} = 5.0$ and 8.0 eV for monolayer GdBr_2 and GdI_2 , respectively) method to investigate the piezoelectric properties of GdX_2 ($X = \text{Br}$ and I) monolayers. The data related to the elastic and piezoelectric properties are

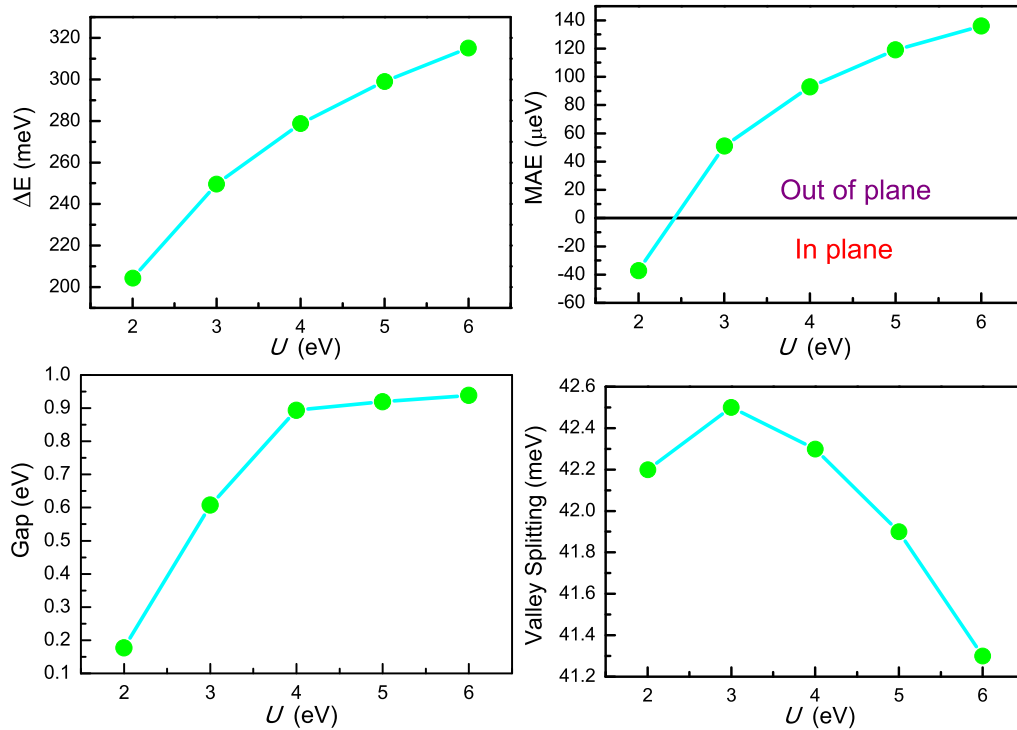


FIG. 10. Top left: The energy difference between the AFM and FM states ΔE . Top right: MAE. Bottom left: Energy band gap. Bottom right: Valley splitting as a function of U for monolayer GdCl_2 .

summarized in Table I. It is found that d_{11} of GdX_2 ($X = \text{Br}$ and I) monolayers are comparable with that of GdCl_2 .

VI. STRAIN EFFECTS

The VBM of unstrained monolayer GdCl_2 is at the Γ point, and it is necessary to tune VBM to the $K/-K$ point using external field for practical applications. As is well known, the strain is a very effective method for tuning the electronic structures of 2D materials [41–47]. a/a_0 is used to simulate the biaxial strain, with a and a_0 being the strained and unstrained lattice constants. In the considered strain range, to confirm the FM ground state, the energy differences of the AFM state with respect to the FM state vs a/a_0 with a rectangular supercell are plotted in Fig. 6. It is found that the energy difference with the biaxial strain varying from 0.94 to 1.06 is always positive and monotonically decreases. This indicates that the ground state of monolayer GdCl_2 is FM in the considered strain range, and the strain can strengthen the FM coupling between Gd atoms from tensile strain to compressive strain. At the applied strain, it is also very important to confirm PMA for stable long-range magnetic ordering without an external field. For the MAE, Fig. 6 shows a decrease with increasing a/a_0 , and the MAE becomes negative with strain over 1.03, which means that the easy axis of monolayer GdCl_2 changes to in plane.

We show only energy band structures of monolayer GdCl_2 (0.94 to 1.02) with PMA by using GGA+SOC in Fig. 7, and the energy band gaps are plotted in Fig. 6. At the applied strain, monolayer GdCl_2 is always an indirect gap semiconductor. It is found that the compressive strain can induce the transition of the VBM from the Γ point to the $K/-K$ point,

which can be observed at a strain of 0.98. In fact, the change in the VBM has been realized at a strain of only 0.99, and the corresponding energy band is plotted in Fig. S1 in the Supplemental Material [48]. The tensile strain can make the CBM change from the M point to a point along the Γ - M path. With a/a_0 from 0.94 to 1.02, the energy band gap first increases and then decreases, which can be observed in many 2D materials [46,47]. As shown in Fig. 6, the valley splitting increases monotonically with increasing a/a_0 . Conversely, a compressive strain decreases the valley splitting, and the valley splitting will become negative at a strain of about 0.963, which implies that the energy of the $-K$ valley is higher than that of the K valley. The Berry curvature distributions of monolayer GdCl_2 with a/a_0 equal to 0.94, 0.98, and 1.02 using GGA+SOC are shown in Fig. 8. It is found that the Berry curvatures (absolute value) of two valleys become large with increasing a/a_0 .

It has been proved that strain engineering can effectively tune the piezoelectric properties of 2D materials [49–52], and next, we investigate the strain effects on the piezoelectric properties of monolayer GdCl_2 . The elastic constants (C_{11} , C_{12} , and $C_{11} - C_{12}$); piezoelectric stress coefficients e_{11} , along with the ionic and electronic contributions; and piezoelectric strain coefficients d_{11} of monolayer GdCl_2 as a function of a/a_0 are plotted in Fig. 9. It is clearly seen that C_{11} , C_{12} , and $C_{11} - C_{12}$ all decrease with strain increasing from 0.94 to 1.02. In the considered strain range, the calculated elastic constants of strained monolayer GdCl_2 satisfy the mechanical stability criteria [30], so they are all mechanically stable. It is found that the strain has little effect on e_{11} , including both the ionic and electronic contributions. However, with

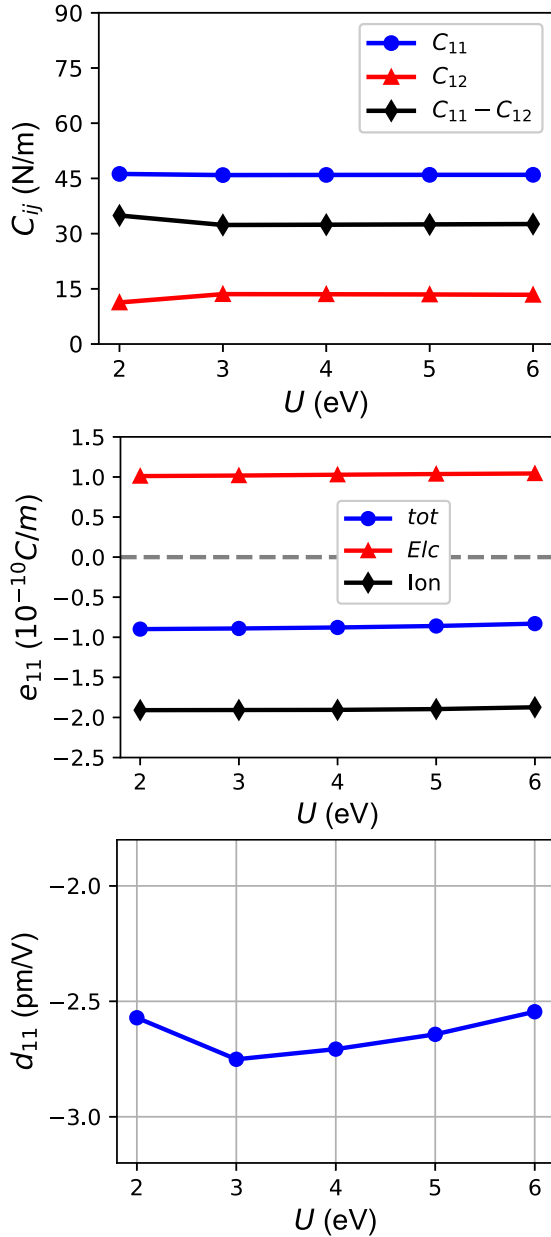


FIG. 11. For monolayer GdCl_2 , the elastic constants C_{ij} ; the piezoelectric stress coefficient e_{11} ; along with the ionic contribution and electronic contribution; and the piezoelectric strain coefficient d_{11} as a function of U .

increasing a/a_0 , d_{11} (absolute value) increases due to the reduced $C_{11} - C_{12}$ based on Fig. 7.

Considering various factors, a very small compressive strain (strain of about 0.99) can make monolayer GdCl_2 a good valley material for realizing the PAVHE, with PMA, a VBM at the $K/-K$ point, strong FM coupling, proper valley splitting, and d_{11} .

VII. ELECTRONIC CORRELATION EFFECTS

To further confirm the reliability of our results, the electronic correlation effects on the magnetic, electronic, and piezoelectric properties of monolayer GdCl_2 are investigated by choosing different U (2–6 eV). The energy differences

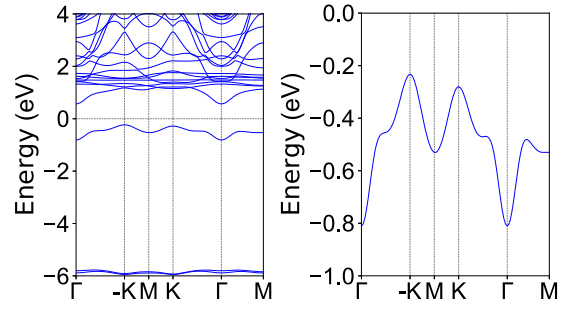


FIG. 12. The band structure of monolayer GdF_2 with SOC for the magnetic moment of Gd along the positive z direction (left), with enlarged views of the valence bands near the Fermi level (right).

between AFM and FM states with a rectangular supercell and MAE vs U are plotted in Fig. 10. With increasing U , the energy difference is always positive and monotonically increases. These characteristics mean that monolayer GdCl_2 always has FM order, and the increasing U can strengthen the FM coupling between Gd atoms. The MAE shows a decrease with decreasing U , and the MAE becomes negative when the easy axis changes to in plane with U less than about 2.5 eV. The energy band structures of monolayer GdCl_2 ($U = 2$ to 6 eV) using GGA+SOC are plotted in Fig. S2 [48], and the energy band gaps and valley splitting are plotted in Fig. 10. When U increases, the VBM is always at the $K/-K$ point, and the gap increases. It is found that the electronic correlation has little influence on valley splitting, and the splitting changes only 1.2 meV with different U (2–6 eV). As shown in Fig. S3 [48], the electronic correlation has little effect on the Berry curvatures of the K and $-K$ valleys. The elastic constants (C_{11} , C_{12} , and $C_{11} - C_{12}$); piezoelectric stress coefficients e_{11} , along with the ionic and electronic contributions; and piezoelectric strain coefficients d_{11} of monolayer GdCl_2 vs U are shown in Fig. 11. The calculated results show that the electronic correlation has a small effect on d_{11} due to its small influence on C_{ij} and e_{11} , and the change is about 0.21 pm/V.

VIII. DISCUSSION AND CONCLUSION

GdX_2 ($X = \text{Cl}, \text{Br}$ and I) monolayers have been predicted [19,20], and the easy axis of monolayer GdCl_2 is along the out-of-plane direction, while monolayer GdBr_2 and GdI_2 possess in-plane magnetic anisotropy. When the compressive strain is larger than 3%, the easy axis of monolayer GdBr_2 changes from in plane to out of plane [20]. This means that monolayer GdF_2 should have PMA due to the small atomic radius of F atoms. For monolayer GdF_2 , the energy difference between AFM and FM states is 0.285 eV, which means that the FM order is the ground state. The optimized lattice constant is 3.465 Å, and the calculated C_{11} and C_{12} are 73.87 and 19.61 N m^{-1} , satisfying the Born criteria of mechanical stability [30]. From Fig. S4 [48], monolayer GdF_2 is dynamically stable due to the missing imaginary frequency. The PMA of monolayer GdF_2 has been confirmed, and the corresponding MAE is 137 μeV per Gd atom. The band structures of monolayer GdF_2 with SOC for the magnetic moment of Gd along the positive z direction are plotted in Fig. 12. Monolayer GdF_2 is an indirect gap semiconductor (0.80 eV) with the VBM at

the $K/-K$ point and the CBM at the Γ point. It was found that the energy of the $-K$ valley is higher than that of the K valley, with valley splitting of 47.6 meV. The calculated Berry curvature distribution of monolayer GdF_2 with SOC for the magnetic moment of Gd along the positive z direction is plotted in Fig. S5 [48]. The absolute values of the Berry curvatures of the K and $-K$ valleys are smaller than those of monolayer GdCl_2 and are no longer identical to the typical valley contrasting properties. Finally, the piezoelectric properties of monolayer GdF_2 were investigated, and the calculated d_{11} is 0.584 pm/V. With respect to GdX_2 ($X = \text{Cl}, \text{Br}, \text{and I}$) monolayers, d_{11} of monolayer GdF_2 becomes positive because the electronic part of monolayer GdF_2 is larger than the ionic part. The related data are summarized in Table I. These results show that monolayer GdF_2 may be a potential valley material for achieving PAVHE.

In summary, a possible method to achieve the anomalous valley Hall effect using the piezoelectric effect was proposed, and then the valleytronic and piezoelectric properties of monolayer GdCl_2 were investigated using the reliable first-principles calculations. Monolayer GdCl_2 is a FM semiconductor with a pair of valleys located at the K and $-K$ points and possess PMA. Arising from the intrinsic magnetic interaction, broken inversion symmetry, and SOC, valley split-

ting can be observed between the K and $-K$ valleys, and the corresponding value is 42.3 meV. The predicted d_{11} is -2.708 pm/V, which can provide a suitable in-plane electric field by uniaxial in-plane strain. Moreover, the effects of strain and electronic correlation on the valley physics and piezoelectric properties were also studied. Finally, a 2D FM semiconductor, GdF_2 , was predicted, which is also a potential ferrovalley material. Monolayer MoS_2 was predicted to be strongly piezoelectric using the first-principles calculations [40], and this was confirmed by experiment [53]. Monolayer $\text{GdCl}_2/\text{GdF}_2$ has the same crystal structure as monolayer MoS_2 , so it is possible to achieve the piezoelectric effect by strain in the $\text{GdCl}_2/\text{GdF}_2$ monolayer and then realize PAVHE. Our work provides an initial idea for realizing and manipulating the valley physics.

ACKNOWLEDGMENTS

This work is supported by Natural Science Basis Research Plan in Shaanxi Province of China (2021JM-456). We are grateful to the Advanced Analysis and Computation Center of China University of Mining and Technology (CUMT) for the award of CPU hours and WIEN2k/VASP software to accomplish this work.

-
- [1] J. R. Schaibley, H. Yu, G. Clark, P. Rivera, J. S. Ross, K. L. Seyler, W. Yao, and X. Xu, *Nat. Rev. Mater.* **1**, 16055 (2016).
- [2] D. Xiao, G. B. Liu, W. Feng, X. Xu, and W. Yao, *Phys. Rev. Lett.* **108**, 196802 (2012).
- [3] S. A. Vitale, D. Nezich, J. O. Varghese, P. Kim, N. Gedik, P. Jarillo-Herrero, D. Xiao, and M. Rothschild, *Small* **14**, 1801483 (2018).
- [4] G. Pacchioni, *Nat. Rev. Mater.* **5**, 480 (2020).
- [5] W. Yao, D. Xiao, and Q. Niu, *Phys. Rev. B* **77**, 235406 (2008).
- [6] D. Xiao, W. Yao, and Q. Niu, *Phys. Rev. Lett.* **99**, 236809 (2007).
- [7] Z. Zhu, A. Collaudin, B. Fauqué, W. Kang, and K. Behnia, *Nat. Phys.* **8**, 89 (2012).
- [8] M. N. Blonsky, H. L. Zhuang, A. K. Singh, and R. G. Hennig, *ACS Nano* **9**, 9885 (2015).
- [9] D. Xiao, M. C. Chang, and Q. Niu, *Rev. Mod. Phys.* **82**, 1959 (2010).
- [10] W. Y. Tong, S. J. Gong, X. Wan, and C. G. Duan, *Nat. Commun.* **7**, 13612 (2016).
- [11] Y. B. Liu, T. Zhang, K. Y. Dou, W. H. Du, R. Peng, Y. Dai, B. B. Huang, and Y. D. Ma, *J. Phys. Chem. Lett.* **12**, 8341 (2021).
- [12] Z. Song, X. Sun, J. Zheng, F. Pan, Y. Hou, M.-H. Yung, J. Yang, and J. Lu, *Nanoscale* **10**, 13986 (2018).
- [13] J. Zhou, Y. P. Feng, and L. Shen, *Phys. Rev. B* **102**, 180407(R) (2020).
- [14] P. Zhao, Y. Ma, C. Lei, H. Wang, B. Huang, and Y. Dai, *Appl. Phys. Lett.* **115**, 261605 (2019).
- [15] X. Y. Feng, X. L. Xu, Z. L. He, R. Peng, Y. Dai, B. B. Huang, and Y. D. Ma, *Phys. Rev. B* **104**, 075421 (2021).
- [16] Y. Zang, Y. Ma, R. Peng, H. Wang, B. Huang, and Y. Dai, *Nano Res.* **14**, 834 (2021).
- [17] R. Peng, Y. Ma, X. Xu, Z. He, B. Huang, and Y. Dai, *Phys. Rev. B* **102**, 035412 (2020).
- [18] W. Du, Y. Ma, R. Peng, H. Wang, B. Huang, and Y. Dai, *J. Mater. Chem. C* **8**, 13220 (2020).
- [19] B. Wang, X. W. Zhang, Y. H. Zhang, S. J. Yuan, Y. L. Guo, S. Dong, and J. L. Wang, *Mater. Horiz.* **7**, 1623 (2020).
- [20] W. Q. Liu, J. W. Tong, L. Deng, B. Yang, G. M. Xie, G. W. Qin, F. B. Tian, and X. M. Zhang, *Mater. Today Phys.* **21**, 100514 (2021).
- [21] H. X. Cheng, J. Zhou, W. Ji, Y. N. Zhang, and Y. P. Feng, *Phys. Rev. B* **103**, 125121 (2021).
- [22] P. Hohenberg and W. Kohn, *Phys. Rev.* **136**, B864 (1964); W. Kohn and L. J. Sham, *ibid.* **140**, A1133 (1965).
- [23] G. Kresse, *J. Non-Cryst. Solids* **192**, 222 (1995).
- [24] G. Kresse and J. Furthmüller, *Comput. Mater. Sci.* **6**, 15 (1996).
- [25] G. Kresse and D. Joubert, *Phys. Rev. B* **59**, 1758 (1999).
- [26] J. P. Perdew, K. Burke, and M. Ernzerhof, *Phys. Rev. Lett.* **77**, 3865 (1996).
- [27] S. L. Dudarev, G. A. Botton, S. Y. Savrasov, C. J. Humphreys, and A. P. Sutton, *Phys. Rev. B* **57**, 1505 (1998).
- [28] X. Wu, D. Vanderbilt, and D. R. Hamann, *Phys. Rev. B* **72**, 035105 (2005).
- [29] A. Togo, F. Oba, and I. Tanaka, *Phys. Rev. B* **78**, 134106 (2008).
- [30] E. Cadelano and L. Colombo, *Phys. Rev. B* **85**, 245434 (2012).
- [31] C. Lee, X. Wei, J. W. Kysar, and J. Hone, *Science* **321**, 385 (2008).
- [32] T. Fukui, Y. Hatsugai, and H. Suzuki, *J. Phys. Soc. Jpn.* **74**, 1674 (2005).
- [33] L. Dong, J. Lou, and V. B. Shenoy, *ACS Nano* **11**, 8242 (2017).
- [34] R. X. Fei, W. B. Li, J. Li, and L. Yang, *Appl. Phys. Lett.* **107**, 173104 (2015).

- [35] Y. Chen, J. Y. Liu, J. B. Yu, Y. G. Guo, and Q. Sun, *Phys. Chem. Chem. Phys.* **21**, 1207 (2019).
- [36] S. D. Guo, Y. T. Zhu, W. Q. Mu, and W. C. Ren, *Europhys. Lett.* **132**, 57002 (2020).
- [37] S. D. Guo, Y. T. Zhu, W. Q. Mu, L. Wang, and X. Q. Chen, *Comput. Mater. Sci.* **188**, 110223 (2021).
- [38] Y. Guo, S. Zhou, Y. Z. Bai, and J. J. Zhao, *Appl. Phys. Lett.* **110**, 163102 (2017).
- [39] W. B. Li and J. Li, *Nano Res.* **8**, 3796 (2015).
- [40] K. N. Duerloo, M. T. Ong, and E. J. Reed, *J. Phys. Chem. Lett.* **3**, 2871 (2012).
- [41] K. L. He, C. Poole, K. F. Mak, and J. Shan, *Nano Lett.* **13**, 2931 (2013).
- [42] H. L. Shi, H. Pan, Y. W. Zhang, and B. I. Yakobson, *Phys. Rev. B* **87**, 155304 (2013).
- [43] T. Cheiwchanhangij, W. R. L. Lambrecht, Y. Song, and H. Dery, *Phys. Rev. B* **88**, 155404 (2013).
- [44] H. Y. Lv, W. J. Lu, D. F. Shao, H. Y. Lub, and Y. P. Sun, *J. Mater. Chem. C* **4**, 4538 (2016).
- [45] H. Peelaers and C. G. Van de Walle, *Phys. Rev. B* **86**, 241401(R) (2012).
- [46] S. D. Guo and J. Dong, *Semicond. Sci. Technol.* **33**, 085003 (2018).
- [47] S. D. Guo, *J. Mater. Chem. C* **4**, 9366 (2016).
- [48] See Supplemental Material at <http://link.aps.org/supplemental/10.1103/PhysRevB.104.224428> for energy band structures, the Berry curvature distribution, and phonon dispersion.
- [49] N. Jena, Dimple, S. D. Behere, and A. D. Sarkar, *J. Phys. Chem. C* **121**, 9181 (2017).
- [50] S. D. Guo, X. S. Guo, Y. Y. Zhang, and K. Luo, *J. Alloy. Compd.* **822**, 153577 (2020).
- [51] Dimple, N. Jena, A. Rawat, R. Ahammed, M. K. Mohanta, and A. D. Sarkar, *J. Mater. Chem. A* **6**, 24885 (2018).
- [52] S. D. Guo, W. Q. Mu, and Y. T. Zhu, *J. Phys. Chem. Solids* **151**, 109896 (2021).
- [53] W. Wu, L. Wang, Y. Li, F. Zhang, L. Lin, S. Niu, D. Chenet, X. Zhang, Y. Hao, T. F. Heinz, J. Hone, and Z. L. Wang, *Nature (London)* **514**, 470 (2014).